IEEE Access
Multidisciplinary | Rapid Review | Open Access Journal

Received 22 July 2022, accepted 1 August 2022, date of publication 8 August 2022, date of current version 18 August 2022.

*Digital Object Identifier 10.1109/ACCESS.2022.3197191*

TOPICAL REVIEW

# Frequency Diverse Array Auto-Scanning Beam Characteristics and Potential Radar Applications

**WEN-QIN WANG, (Senior Member, IEEE)**
Yangtze Delta Region Institute (Huzhou), University of Electronic Science and Technology of China, Huzhou 313001, China
School of Information and Communication Engineering, University of Electronic Science and Technology of China, Chengdu 611731, China
e-mail: wqwang@uestc.edu.cn

**ABSTRACT** Different from the phased-array with the same carrier frequency for all elements providing only angle-dependent beampattern, frequency diverse array (FDA) using a small frequency offset across its array elements offers new application capabilities due to its both angle and range dependent beampattern, which allows auto beam-scanning capability even without the employment of phase shifters, which are required in phased-array. This paper studied FDA auto-scanning beam characteristics and several potential radar applications. The FDA auto-scanning beam characteristics including range and angle coupling, beam auto-scanning rate and integral array again are analyzed. To fully utilize FDA specific auto-scanning beam characteristics, several potential applications such as radio frequency (RF) stealth or RF localization deception, range-ambiguous clutter suppression and mainlobe interference suppression are discussed. Moreover, several discussions about space-time adaptive processing and possible future investigations are provided. This paper is formulated from a top-level system description, which aims to introduce this promising FDA technique to radar community so that more investigations can be facilitated.

**INDEX TERMS** Frequency diverse array (FDA), auto-scanning antenna, radio frequency (RF) stealth, time-variant beampattern, space-time adaptive processing, ambiguous clutter suppression, mainlobe interference suppression.

## I. INTRODUCTION

Beam-scanning antenna is a key requirement in many wireless systems [1]. Since mechanically beam-scanning reflector antenna has slow speed of beam scanning, typical solution is to adopt phased-array antenna [2]. Phased-array is well known for its robust capability to electronically steer its beam with high effectiveness [3], [4], the beam steering of phased-arrays in an angle is fixed for all range cells [5], [6]. That is, a limitation of the phased-array antenna is that the beam steering is independent of the range parameter. However, the ability to allow range-dependent beampattern control is an increasingly desirable capability in many applications [7], such as range ambiguous clutter or interference suppression. On the other hand, low-cost beam-scanning antennas are very promising for mobile terminals [8], [9], [10].

The associate editor coordinating the review of this manuscript and approving it for publication was Debdeep Sarkar.

In this paper, frequency diverse array (FDA) [11] is adopted to study for low-cost wide-angle beam auto-scanning antennas. As illustrated in Figure 1, different from the phased-array with the same carrier frequency for all elements, which provides only angle-dependent beampattern, FDA using small frequency offsets across its array elements enables the beampattern focusing direction to change as a function of the angle, range and even time variables [12]. FDA can be seen as a combination of spatial diversity and frequency diversity. Nevertheless, note that FDA is different from traditional multiple-input multiple-output (MIMO), orthogonal frequency division multiplexing (OFDM) and frequency scanning techniques. The comparisons between FDA and other similar array techniques such as phased-array, MIMO, frequency scanning and time-modulated arrays are listed in Table 1. It is shown that, while compared with traditional phased-array offers only angle-dependent beampattern, FDA provides not only angle-dependent but also range-dependent beampattern which is an advantage for

**TABLE 1. Comparisons between FDA and several representative arrays.**

| array name | subcarriers | transmitted signals | array gain | transmit beampattern | |
|---|---|---|---|---|---|
| | | | | range-dependent | angle-dependent |
| FDA | non-orthogonal | coherent | √ | √ | √ |
| phased-array | non-orthogonal | coherent | √ | | √ |
| MIMO-OFDM | orthogonal | non-coherent | | | √ |
| colocated MIMO | same carrier | non-coherent | | | √ |
| frequency-scanning | same carrier | coherent | √ | | √ |
| time-modulated | same carrier | coherent | √ | | √ |

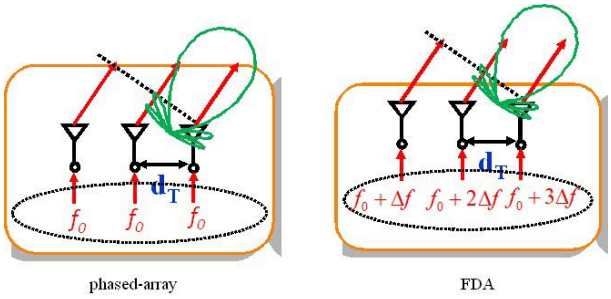


**FIGURE 1. Difference between phased-array and FDA antennas.**

range-dependent target localization and interference suppression, but FDA also has the disadvantage of range-angle coupling beampattern response, which may result in ambiguous results for joint range and angle estimation of targets.

Motivated by its range-dependent/time-variant beampattern characteristics and promising application potentials [13], a special issue about FDA was published in IEEE Journal of Selected Topics in Signal Processing [14]. In recent years, FDA has received much attention, such as beampattern synthesis, range-dependent interference suppression, radar target detection and localization, deceptive jamming [15], [16], [17], secure communications [18], and high-resolution imaging.

The FDA range-dependent transmit beamapattern characteristics for a monochromatic continuous-wave waveform were analyzed in multiple papers [19], [20]. The angle and time periodicity of FDA transmit beampattern was analyzed in [21] and electromagnetically simulated in [22]. Furthermore, the multipath propagation characteristics of FDA transmitted signals were analyzed in [23]. Since the FDA with uniformly spaced linear elements and linearly progressive frequency offsets will generate range-angle coupling S-shaped beampattern, multiple methods including nonlinearly increasing [24], random [25], [26] and time-dependent [27], [28], [26], [29] frequency offsets were studied to decouple for focusing beampattern synthesis. However, it should be noted that the essence of time-variance in FDA transmit beampattern is ignored in the aforementioned papers by only considering an instantaneous time. That is to say, time-invariant beampattern cannot be implemented for practical FDA antenna [30]. Otherwise, it just simplifies into a traditional phased-array antenna. Nevertheless, we believe that FDA beampattern time-variance should be utilized for enhanced application performance, rather than suppressing the time-variance. Therefore, unlike the FDA literature that mainly suppress transmit beampattern time-variance, this paper analyzes and exploits FDA time-variance to provide wide-angle auto-scanning beam for potential radio frequency (RF) stealth, range-ambiguous clutter suppression and mainlobe interference suppression applications.

The main contributions of this paper are summarized as follows:

- The auto-scanning beam characteristics of FDA antennas together with the time-variance, range-dependence, range and angle coupling, and integral array gain characteristics are systematically analyzed and compared with traditional phased-array antenna.
- FDA potential radar applications including RF stealth or RF localization deception, range-ambiguous clutter suppression and mainlobe interference suppression are presented, which shows outperformed performance over classic phased-array techniques.
- Several discussions about technical challenges in FDA radar space-time adaptive processing and possible future investigations are provided from a top-level system description to call for more investigations on such promising FDA techniques.

The remaining sections are organized as follows: Section II analyzes the auto-scanning characteristics of FDA transmit beam. Section III discusses FDA potential applications including RF localization deception and mainlobe interference suppression. Furthermore, several discussions and possible future investigations are provided in Section IV. Finally, conclusions are drawn in Section V.

## II. FDA AUTO-SCANNING BEAM CHARACTERISTICS

### A. GENERAL FDA TRANSMIT BEAMPATTERN

We consider a general uniform linear array (ULA) FDA, which modulates the same baseband waveform to a distinct center frequency for each array element. As shown in Figure 2, the $m$th array element transmits the signal at the center frequency:

$$f_m = f_0 + \Delta f_m, \quad m = 0, 1, \ldots, M-1 \tag{1}$$

where $f_0$ is the carrier frequency and $\Delta f_m$ is the frequency offset for the $m$th element. In amplitude sense, the propagation attenuation for the distance differences between individual elements to the given position point can be ignored. In phase

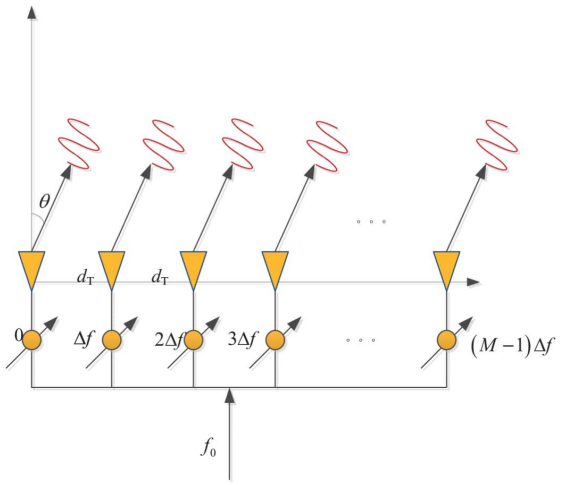


**FIGURE 2.** Illustration of FDA transmitter.

sense, the range $r_m$ from the observation point to the $m$th element can be approximated by $r_m \approx r - md\sin\theta$, where $r$ is the reference range to the first element, $d$ is the element spacing, which is assumed to be $d = c_0/2f_0$ with $c_0$ being the speed of light, and $\theta$ is the array direction angle. The typical $\Delta f_m$ in an FDA radar system with the carrier frequency of $f_0 = 10$ GHz is about $\Delta f_m = 10$ kHz. That is, $\Delta f < f_0/10^6$ is generally adopted. Therefore, due to the fact that $f_0 \gg \Delta f_m$, the equal normalized electric field function $e(\theta)$ is assumed for all elements.

Generally, consider a pulsed FDA system and define the transmitted baseband waveform $\phi(t)$, $0 \le t \le T_p$ with pulse duration $T_p$ satisfies the unit energy, i.e., $\int_{T_p} \phi^*(t)\phi(t)\mathrm{d}t = 1$, where $^*$ denotes the complex conjugate operator. For a given far-field position with angle $\theta$ and range $r$, the arrived signals can be expressed as

$$s(t) = \frac{e(\theta)}{r} e^{j2\pi f_0\left(t-\frac{r}{c_0}\right)} \sum_{m=0}^{M-1} w_m^* \phi\left(t - \frac{r_m}{c_0}\right) \times e^{j\left(2\pi\Delta f_m\left(t-\frac{r}{c_0}\right)+m2\pi f_0\frac{d\sin\theta}{c_0}+\frac{m2\pi\Delta f_m d\sin\theta}{c_0}\right)} \quad (2)$$

where $w_m$ is the complex weight for the $m$th element. Note that, here the time variable $t$ should be limited by $\frac{r}{c_0} \le t \le T_p + \frac{r}{c_0}$. For notation convenience, we define

$$\gamma_m = 2\pi\Delta f_m\left(t - \frac{r}{c_0}\right) + m2\pi f_0\frac{d\sin\theta}{c_0} + \frac{m2\pi\Delta f_m d\sin\theta}{c_0} \quad (3)$$

Under narrow-band assumption, we have $\phi\left(t - \frac{r_m}{c_0}\right) \approx \phi\left(t - \frac{r}{c_0}\right)$. In this case, the FDA transmit beampattern can be defined as

$$P(\theta, r, t) = \begin{cases} \left|\sum_{m=0}^{M-1} e^{j\gamma_m}\right|, & \frac{r}{c_0} \le t \le T_p + \frac{r}{c_0} \\ 0, & \text{otherwise} \end{cases} \quad (4)$$

Since $\gamma_m$ depends on both the angle $\theta$ and range $r$, the FDA transmit beampattern $F(\theta, r, t)$ will change as a function of the angle $\theta$ and/or range $r$. For instance, the beampattern $P(\theta, r, t)$ for given range $r_0$ and time $t_0$ can be expressed, respectively, as [6]

$$P(\theta, r_0, t) = \left|\sum_{m=0}^{M-1} e^{j\gamma_m}\right|, \quad \frac{r_0}{c_0} \le t \le T_p + \frac{r_0}{c_0} \quad (5a)$$

$$P(\theta, r, t_0) = \left|\sum_{m=0}^{M-1} e^{j\gamma_m}\right|, \quad c_0 t_0 \le r \le c_0(t_0 + T_p) \quad (5b)$$

As an example, consider an FDA with $M = 16$ elements spaced by half wavelength and $T_p = 10\mu s$. For simplicity without loss of generality, $\Delta f_m = m \cdot \Delta f$ with $\Delta f$ being a constant is assumed. Figure 3 shows that FDA beam will change as a function of the time (range) for a fixed range (time), which implies that FDA transmit beam will auto-scan in the range-angle dimension even for fixed range and/or time. This motivates us to adopt FDA for wide-angle auto-scanning beam applications.

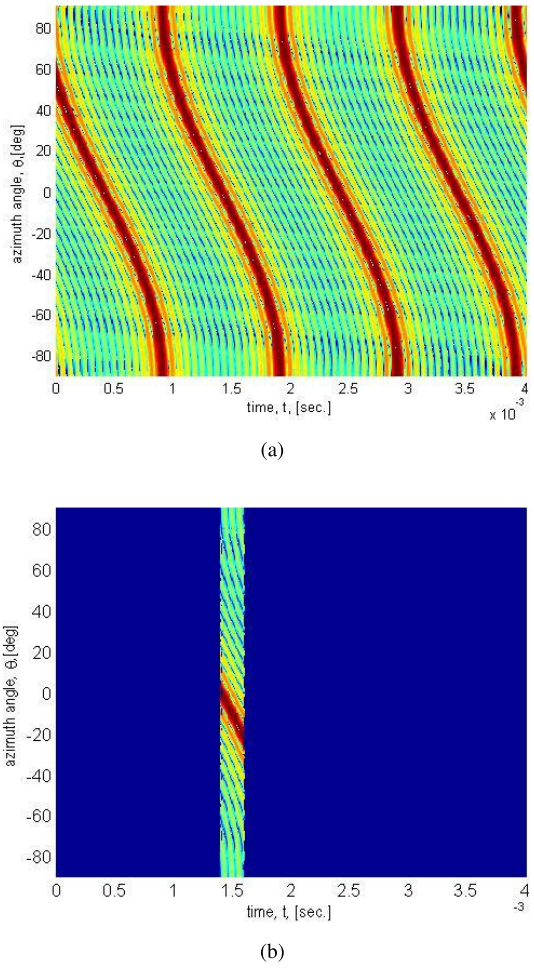


**FIGURE 3.** Beampattern comparisons of same FDA under continuous-wave and pulsed transmissions at a given range 120*km* with $M = 16$ and $\Delta f = 1$ kHz: (a) Continuous-FDA, (b) Pulsed-FDA.

### B. FDA RANGE AND ANGLE COUPLING BEAMPATTERN

To quantitatively analyze the specified FDA beampattern characteristics and for simplicity without loss of generality, $\Delta f_m = m \cdot \Delta f$ with $\Delta f$ being a constant is assumed thereafter. Considering (3), due to the fact that $\Delta f_m \ll c_0$ and $m = 0, 1, 2, \ldots, M-1$ is generally smaller than 100, we then have the following approximation:

$$\frac{m2\pi\,\Delta f_m d\sin\theta}{c_0} = \frac{m^2 2\pi\,\Delta f d\sin\theta}{c_0} \approx \frac{m2\pi\,\Delta f d\sin\theta}{c_0} \tag{6}$$

which is true because both left-side and right-side are nearly 0 and thus they depend very weakly on $m$. The (3) can then be further approximated as

$$\gamma_m = m2\pi\,\Delta f\left(t - \frac{r}{c_0}\right) + m2\pi f_0 \frac{d\sin\theta}{c_0} + \frac{m2\pi\,\Delta f d\sin\theta}{c_0} \tag{7}$$

In this case, substituting (7) into (4) yields the FDA transmit beampattern:

$$P(\theta, r, t) = \left|\frac{\sin\left(M\pi\left(\Delta f t - \frac{f_0}{c_0}r + \frac{f_0}{c_0}d\sin\theta + \frac{\Delta f}{c_0}d\sin\theta\right)\right)}{\sin\left(\pi\left(\Delta f t - \frac{f_0}{c_0}r + \frac{f_0}{c_0}d\sin\theta + \frac{\Delta f}{c_0}d\sin\theta\right)\right)}\right| \tag{8}$$

The FDA beampattern maximum arrives at

$$\Delta f\left(t - \frac{r}{c_0}\right) + f_0\frac{d\sin\theta}{c_0} + \frac{\Delta f d\sin\theta}{c_0} = n, \quad n = 0, 1, 2, \ldots \tag{9}$$

Even for a fixed time $t = 0$, the beampattern peaks will be periodic, which arrive at

$$\theta_{\text{peak}} = \sin^{-1}\left(\frac{c_0 n + \Delta f r}{(f_0 + \Delta f)d}\right), \quad n = 0, 1, 2, \ldots \tag{10}$$

with $\lambda_0 = c_0/f_0$ being the wavelength, which is generally assumed to be $d = \lambda_0/2$. As shown in Figure 4, due to the range-angle coupling effects, the "S" peaks will be generated in the FDA range-angle beampattern.

### C. FDA BEAM AUTO-SCANNING RATE

It should be noted that, for a given pair $(\theta, r)$, the above (10) does not guarantee the existence of beampattern maximum, because the suitable integer $n$ may not exist. The FDA beam auto-scanning rate can be evaluated by differentiating (9) with respect to $t$:

$$\frac{\mathrm{d}\theta}{\mathrm{d}t} = -\frac{c_0 \cdot \Delta f}{(f_0 + \Delta f)\, d\cos\theta} \tag{11}$$

It states the beam scanning rate depends on both angle $\theta$ and frequency offset $\Delta f$.

Suppose the corresponding angles at $t_1$ and $t_2$ are $\theta_1$ and $\theta_2$, respectively. The FDA beam scanning during one pulse duration $T_p$ will be

$$\sin\theta_1 - \sin\theta_2 = \frac{c_0\Delta f\,(t_2 - t_1)}{(f_0 + \Delta f)\,d} = \frac{c_0\Delta f T_p}{(f_0 + \Delta f)\,d} \tag{12}$$

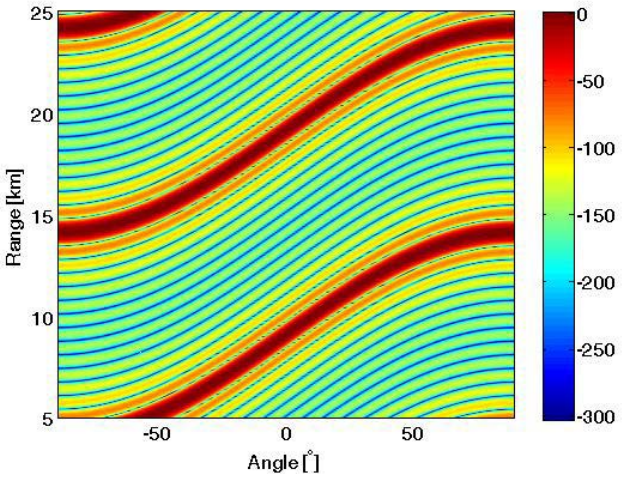


**FIGURE 4.** FDA range-angle coupling transmit beampattern: $M = 16$, $f_0 = 10$ GHz, and $\Delta f = 10$ kHz.

This implies that FDA can complete the entire scanning from $-90°$ to $90°$ for given $\Delta f$ and $T_p$. Generally, $d = c_0/(2f_0)$ is adopted. In this case, the above (12) can be simplified into

$$\sin\theta_1 - \sin\theta_2 = \frac{2f_0\Delta f T_p}{(f_0 + \Delta f)} \approx 2\Delta f T_p \tag{13}$$

If $\Delta f = 1/T_p$, the beam can scan from $-90°$ to $90°$ in one pulse. However, the beam direction change in one pulse will be ignorable for $1/\Delta f \gg T_p$. Figure 5 shows the FDA beam scanning in one pulse duration and across the pulses. That is, the actual beam scanning characteristics can be controlled by tuning the frequency offset, even for a fixed element spacing in the antenna without changes of the pulse duration $T_p$ and carrier frequency $f_0$. However, it should be noted that the radiation pattern may be not an ideal "S" shape in the pulsed FDA systems.

### D. FDA INTEGRAL ARRAY GAIN

Since FDA beampattern has time-variance and auto-scanning characteristics, to effectively evaluate the time-variant array gain, we define the integral transmit beampattern in the angle dimension as [31]

$$\text{IP}(\theta) = \left|\mathbf{a}_\theta^H(\theta)\,\mathbf{R}_T^T\mathbf{a}_\theta(\theta)\right| \tag{14}$$

where $^H$ is the conjugate transpose operator, $\mathbf{a}_\theta(\theta)$ is the FDA transmit steering vector in the angle dimension:

$$\mathbf{a}_\theta(\theta) = \left[1\ e^{j2\pi\frac{d}{\lambda_0}\sin\theta}\ \ldots\ e^{j2\pi(M-1)\frac{d}{\lambda_0}\sin\theta}\right]^T \tag{15}$$

with $^T$ being the transpose operator, and $\mathbf{R}_T \in \mathcal{C}^{M\times M}$ is the covariance matrix of the FDA transmitted signal with the $(m, m')$th element being

$$[\mathbf{R}_T]_{m,m'} = \int_{T_p}\left(w_m\phi(t)e^{j2\pi m\Delta f t}\right)\left(w_{m'}\phi(t)e^{j2\pi m'\Delta f t}\right)^* \mathrm{d}t \tag{16}$$

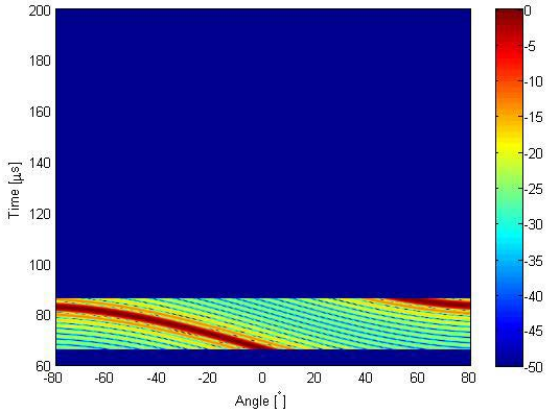


(a)

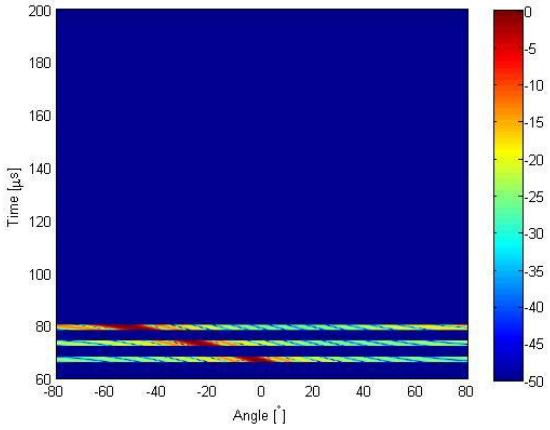


(b)

**FIGURE 5.** FDA beam scanning with $M = 16$ and $\Delta f = 30$ kHz: (a) in one pulse, (b) across the pulses.

where $w_m$ and $w_{m'}$ denote the weights for the $m$th and $m'$th elements, respectively.

As shown in Figure 6, if $\Delta f \ll B_s$, where $B_s$ is the baseband signal bandwidth, $[\mathbf{R}_T]_{m,m'} \approx w_m w_{m'}^*$, and then $\mathrm{IP}(\theta) \approx \left|\mathbf{w}^T \mathbf{a}_\theta(\theta)\right|$, with $\mathbf{w} = [w_0\ w_1\ \ldots\ w_{M-1}]^T$ being the transmit weighting vector. In this case, the FDA will have equal array gain to conventional phased array. In contrast, if $\Delta f \geq B_s$, then $[\mathbf{R}_T]_{m,m'} \approx 0$ and $\mathrm{IP}(\theta) \approx \|\mathbf{w}\|^2$, where $\|\mathbf{w}\|$ is the 2-norm operator. This case implies that orthogonal baseband waveforms are employed by the FDA and omnidirectional array radiation will generate for the array antenna.

## III. POTENTIAL APPLICATIONS

FDA has not only all the advantages of phased-array, but also the range-dependence, range-angle coupling and spatial variance characteristics in the transmit beampattern. It is thus expected to have a subversive impact on the existing active radar target detection, passive detection and electronic countermeasure techniques. In this section, we discuss several typical potential applications.

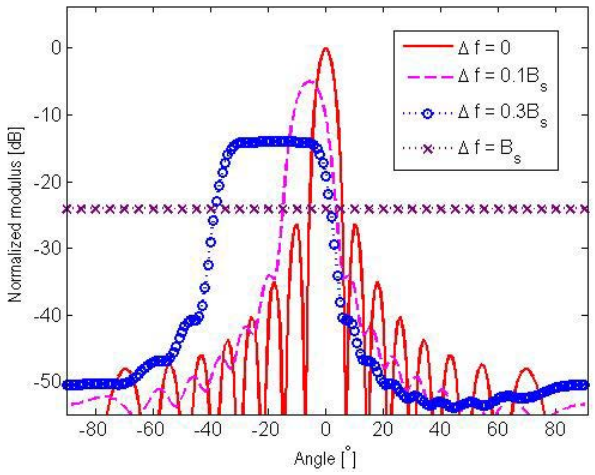


**FIGURE 6.** FDA integral transmit beampattern with $M = 16$, $f_0 = 10$ GHz.

### A. RF LOCALIZATION DECEPTION

According to (8), FDA will generate an apparent angle $\theta_a$ [19]:

$$\theta_a = \arcsin\left(\frac{c_0 \Delta f t}{2\pi f_0 d} + \sin\theta + \frac{\Delta f \sin\theta}{f_0} + \frac{\Delta f r}{f_0 d}\right) \quad (17)$$

which is different from its real scanning angle $\theta$, as shown in Figure 7 that FDA apparent direction angle is not equal to its physical direction angle. That is, the FDA apparent direction depends on not only its physical direction but also the employed frequency offset $\Delta f$. This implies that FDA transmitted signals may have RF localization deception or RF stealth for low probability of identification (LPI) applications [32].

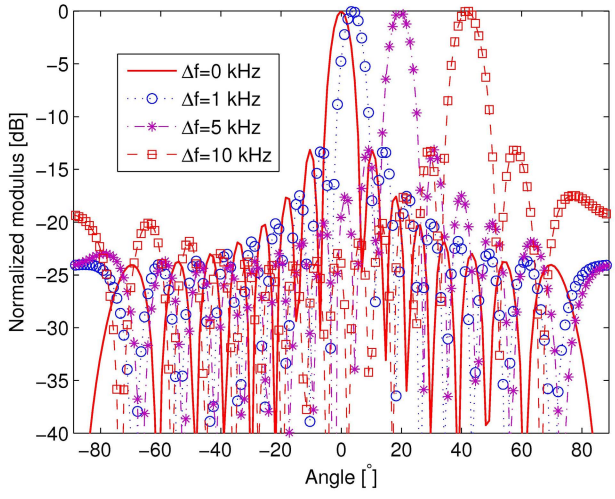


**FIGURE 7.** FDA apparent direction angle and physical direction angle, which the physical direction angle is $\theta = 0°$.

To evaluate the RF localization deception performance of the FDA transmitted signals, we consider one four-antenna reconnaissance receiver, as shown in Figure 8. The

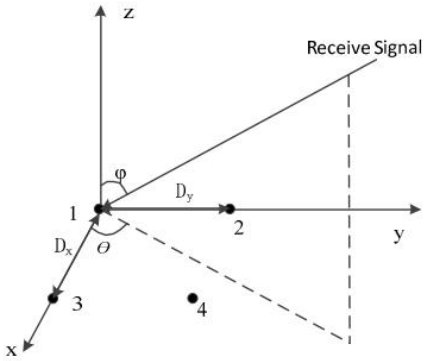


**FIGURE 8.** Illustration of four-antenna reconnaissance receiver.

antennas 1 and 3 are placed along the $x$-axis with spacing $D_x$ and the antennas 1 and 2 are placed along the $y$-axis with spacing $D_y$. Suppose the incoming FDA signals have the elevation angle $\varphi$ and azimuth angle $\theta$.

Suppose the slant range from the reconnaissance receiver to the antenna 1 is $r$. According to (2), the four antennas received signals can be expressed, respectively, as

$$\begin{aligned} & y_1(\theta, r, t) \\ &= \frac{\exp(j\phi_0)}{r} \cdot \sum_{m=0}^{M-1} \exp\left\{-j2\pi m\left(\Delta f t - \frac{\Delta f r}{c_0} - \frac{d\sin\theta}{\lambda_0}\right)\right\} \\ &= \frac{\exp\left\{j\left[\phi_c + \pi(M-1)\frac{d\sin\theta}{\lambda_0}\right]\right\}}{r} \\ &\quad \cdot \frac{\sin\left[\pi M\left(\Delta f t - \frac{\Delta f r}{c_0} - \frac{d\sin\theta}{\lambda_0}\right)\right]}{\sin\left[\pi M\left(\Delta f t - \frac{\Delta f r}{c_0} - \frac{d\sin\theta}{\lambda_0}\right)\right]} \end{aligned} \tag{18}$$

$$\begin{aligned} & y_2(\theta, r, t) \\ &= \frac{1}{r}\sum_{m=0}^{M-1} \exp\{-j2\pi\,(f_0 + m\Delta f) \cdot \left(t - \frac{r + md\sin\theta - D_y\sin\theta}{c_0}\right)\} \\ &= \frac{\exp(j\phi_0)}{r}\sum_{M=0}^{M-1} \exp \times \left\{-2\pi m\left(\Delta f t - \frac{\Delta f r}{c_0} - \frac{d\sin\theta}{\lambda_0}\right)\right. \\ &\quad \left. \times\ -j2\pi\left(\frac{D_y\sin\theta}{\lambda_0} + m\Delta f\frac{D_y\sin\theta}{c_0}\right)\right\} \end{aligned} \tag{19}$$

$$\begin{aligned} & y_3(\theta, r, t) \\ &= \exp\left[j\left(\phi_0 - 2\pi\frac{D_x\cos\theta}{\lambda_0}\right)\right] \cdot \sum_{m=0}^{M-1} \exp\left\{-j2\pi m\left(\Delta f t - \frac{\Delta f r}{c_0} - \frac{d\sin\theta}{\lambda_0}\right)\right\} \\ &= \frac{\exp\left\{j\left[\phi_c + \pi(M-1)\frac{d\sin\theta}{\lambda_0} - 2\pi\frac{D_x\cos\theta}{\lambda_0}\right]\right\}}{r} \\ &\quad \cdot \frac{\sin\left[\pi M\left(\Delta f t - \frac{\Delta f r}{c_0} - \frac{d\sin\theta}{\lambda_0}\right)\right]}{\sin\left[\pi\left(\Delta f t - \frac{\Delta f r}{c_0} - \frac{d\sin\theta}{\lambda_0}\right)\right]} \end{aligned} \tag{20}$$

$$\begin{aligned} & y_4(\theta, r, t) \\ &= \frac{\exp\left\{j\left[\phi_0 - 2\pi\left(\frac{D_y\sin\theta}{\lambda_0} + \frac{D_x\cos\theta}{\lambda_0}\right)\right]\right\}}{r} \cdot \sum_{m=0}^{M-1} \exp\left\{-j2\pi m\left(\Delta f t - \frac{\Delta f r}{c_0} - \frac{d\sin\theta}{\lambda_0}\right)\right\} \\ &= \frac{\exp\left\{j\left[\phi_c + \pi(M-1)\frac{d\sin\theta}{\lambda_0} - 2\pi\left(\frac{D_y\sin\theta}{\lambda_0} + \frac{D_x\cos\theta}{\lambda_0}\right)\right]\right\}}{r} \\ &\quad \cdot \frac{\sin\left[\pi M\left(\Delta f t - \frac{\Delta f r}{c_0} - \frac{d\sin\theta}{\lambda_0}\right)\right]}{\sin\left[\pi\left(\Delta f t - \frac{\Delta f r}{c_0} - \frac{d\sin\theta}{\lambda_0}\right)\right]} \end{aligned} \tag{21}$$

where $\phi_0$ is the reference initial phase. Taking the signals received by the antenna 1 as the reference and assuming the carrier phases of $y_1(\theta, r, t)$, $y_2(\theta, r, t)$, $y_3(\theta, r, t)$ and $y_4(\theta, r, t)$ are $\phi_1$, $\phi_2$, $\phi_3$ and $\phi_4$, the phase differences between the four received signals to the antenna 1 can be calculated as

$$\Delta\phi_2 = \phi_2 - \phi_1 = -\frac{2\pi D_y\sin\theta}{\lambda_0} \tag{22a}$$

$$\Delta\phi_3 = \phi_3 - \phi_1 = -\frac{2\pi D_x\cos\theta}{\lambda_0} \tag{22b}$$

$$\begin{aligned} \Delta\phi_4 &= \phi_4 - \phi_1 = \frac{2\pi D_y\sin\theta}{\lambda_0} - \frac{2\pi D_x\cos\theta}{\lambda_0} \\ &= \Delta\phi_2 + \Delta\phi_3 \end{aligned} \tag{22c}$$

The direction of arrival (DOA) of the FDA transmitted signal can then be estimated from the interferometry phase as

$$\hat{\theta} = \arctan\left(\frac{\Delta\phi_2 \cdot D_x}{\Delta\phi_3 \cdot D_y}\right) \tag{23}$$

As an example, we consider the following parameters: $D_x = 0.015m$, $D_y = 0.0075m$, $f_0 = 10$ GHz, $\Delta f = 20$ kHz and $M = 16$ elements spaced by half wavelength, Figure 9 compares the four-antenna receiver's interferometry reconnaissance performance for FDA and phased-array transmitted signals under SNR $= 15$ dB. The results verify that, while compared to phased-array, FDA will seriously degrade the interferometry reconnaissance performance, which validates that RF localization deception capability indeed can be achieved for the FDA transmitted signals.

### B. RANGE AMBIGUOUS CLUTTER SUPPRESSION

Since FDA transmit steering vector depends on the angle, range and time variables, it is necessary to adopt space-time-range joint processing [33] for FDA radar data processing. In [34], a range-angle coupled signal model for simultaneous adaptation in the spatial and range dimensions was utilized to mitigate the joint space-range sidelobes inherent

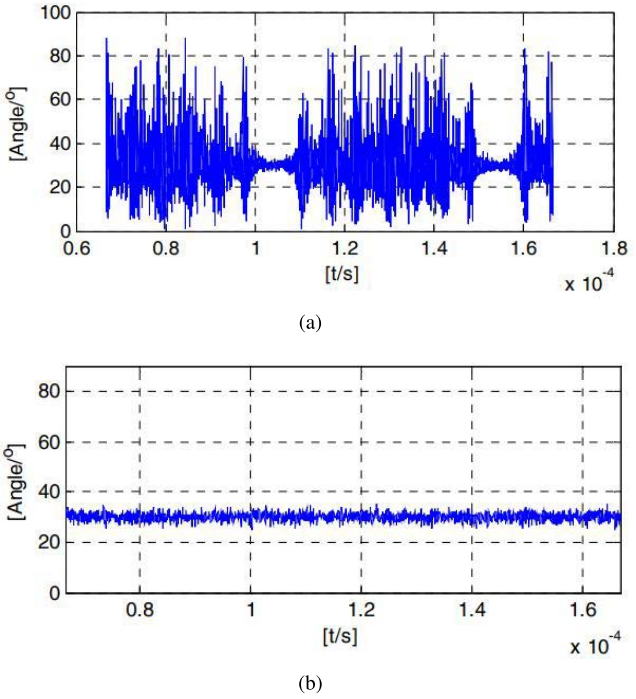


**FIGURE 9.** RF reconnaissance performance comparison between FDA and phased-array: (a) FDA transmitted signals, (b) phased-array transmitted signals.

to FDA radars. A reiterative minimum mean square error-based space-time adaptive processing (STAP) algorithm was proposed in [35] to address FDA radar range-couple adaptive processing. Additionally, Xu *et al.* [36] studied robust adaptive beamforming for FDA-STAP radar fast-moving target detection and Wen *et al.* [37], [38] investigated STAP in slow-time FDA-MIMO radars.

Particularly, STAP for range ambiguous clutter suppression in airborne FDA-MIMO radar was presented in [39] by exploiting the range dependence property and relationship between spatial and Doppler frequencies. Due to the fact that FDA steering vector consists of the angular, range and time variables, the spatial frequency of the forward-looking FDA radar with azimuth angle $\theta$ and elevation angle $\varphi$ should be formulated as

$$f_s = -\frac{2\Delta f r}{c_0} + \frac{d}{\lambda_0}\sin\theta\cdot\cos\varphi \tag{24}$$

The above (24) simplifies into the spatial frequency for phased-array forward-looking radar when $\Delta f = 0$, which states that FDA radar produces both angle and range dependent spatial frequency, while only angle dependent spatial frequency can be generated in phased-array radar.

Consider also the Doppler frequency

$$f_d = \frac{2v}{\lambda_0 f_{\text{prf}}}\cos\theta\cdot\cos\varphi \tag{25}$$

where $f_{\text{prf}}$ is the pulse repetition frequency (PRF) and $v$ is the relative velocity between the radar platform and observed target. The spatial and Doppler frequencies relationship in the FDA radar can then be expressed as [39]

$$\left(\frac{\lambda_0}{d}(f_s - f_r)\right)^2 + \left(\frac{\lambda_0 f_{\text{prf}}}{2v} f_d\right)^2 = \cos^2\varphi \tag{26}$$

Obviously, this elliptical relationship is different from that of the phased-array radar [40]. It was concluded in [39] that the elliptical curves in forward-looking FDA radar will be shifted in the spatial frequency domain with respect to the slant range while that of traditional phased-array radar will remain invariant. This implies that the clutters from ambiguous and unambiguous ranges cannot be separated in phased-array radar STAP processing, but they can be discriminated in the STAP spatial frequency domain for FDA radar.

To evaluate the STAP performance of FDA radar, we consider the system improvement ratio (SIR), which is defined as [41]

$$\text{SIR} = \frac{P_s^{\text{out}}/P_n^{\text{out}}}{P_s^{\text{in}}/P_n^{\text{in}}} = \frac{\mathbf{w}^*\mathbf{s}\mathbf{s}^*\mathbf{w}\cdot\text{Tr}(\mathbf{R})}{\mathbf{w}^*\mathbf{R}^*\mathbf{w}\cdot\mathbf{s}^*\mathbf{s}} \tag{27}$$

where $P_s^{\text{in}}/P_s^{\text{out}}$ and $P_n^{\text{in}}/P_n^{\text{out}}$ denote the signal and noise (and clutter) input/output power, $\mathbf{w}$ is the space-time adaptive weighting vector, $\mathbf{s}$ is the assumed steering vector for a target, $\mathbf{R}$ is the clutter-plus-noise covariance matrix, and $\text{Tr}(\cdot)$ denotes the trace of a matrix. According to the SIR, the minimum detectable Doppler frequencies at two sides of the clutter notch can then be determined, respectively, as

$$\text{MDD}_+ = \min_{f_d} f_d, \quad s.t.\ L_{\text{SIR}} \geq L_0, \quad f_d > 0 \tag{28}$$

$$\text{MDD}_- = \min_{f_d} f_d, \quad s.t.\ L_{\text{SIR}} \geq L_0, \quad f_d < 0 \tag{29}$$

where $L_{\text{SIR}} = \text{SIR}/\gamma_0$ with $\gamma_0$ being the coherent accumulation gain, and $L_0$ is the decision threshold. Defining the Doppler frequency at the clutter notch as $f_d = 0$, the normalized minimum detectable Doppler frequency can then be defined as

$$\text{MDD} = \frac{1}{2}(\text{MDD}_+ - \text{MDD}_-) \tag{30}$$

Considering the forward-looking FDA radar system with $M = 8$ transmit elements and $N = 8$ receive elements spaced by half wavelength and the other parameters are listed as $f_0 = 8$ GHz, $\Delta f = 3$ kHz, PRF $= 15$ kHz, platform altitude is 3 km, platform velocity is $v = 90$ m/s, signal-to-noise ratio (SNR) is 0 dB, clutter-to-noise ratio (CNR) is 20 dB, and 10 snapshots are assumed, Figure 10 compares the FDA radar SIR loss versus normalized Doppler frequency with that of the phased-array with the same parameters except $\Delta f = 0$ Hz, where the cases without and with range ambiguity are considered separately. Note that the decision threshold is typically considered at $-2$ dB in statistical detection algorithms [41]. The results show that narrower notch width can be achieved for the FDA radar, which states that smaller minimum detectable velocity can be implemented for FDA radar than traditional phased-array radar, because the detectable velocity has a linear relationship to the minimum detectable

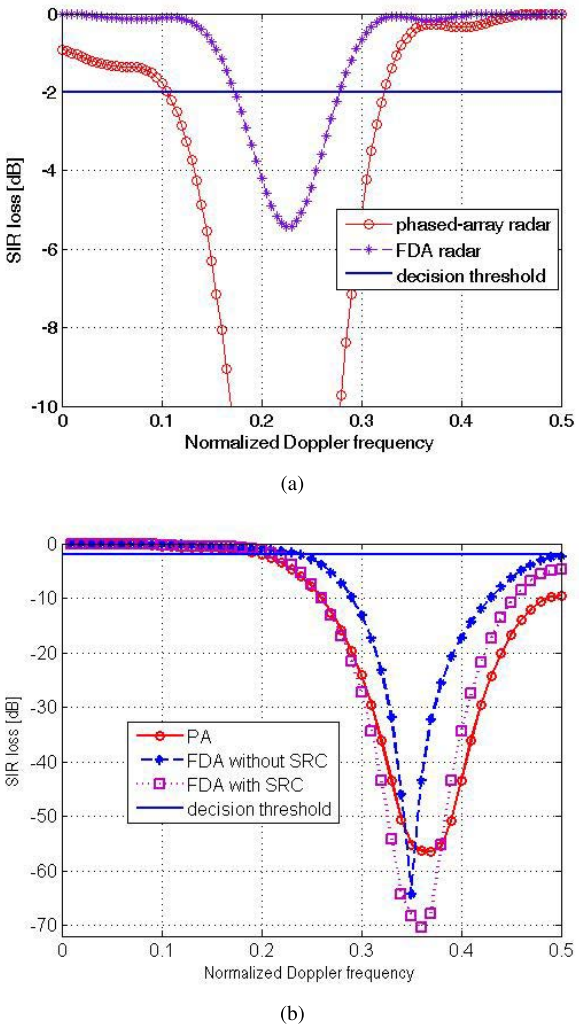


**FIGURE 10.** Forward-looking FDA radar SIR loss versus normalized Doppler frequency: (a) without range ambiguity, (b) with range ambiguity.

Doppler frequency in moving target indication (MTI) applications.

### C. MAINLOBE JAMMING SUPPRESSION

It is well known that phased-array can effectively suppress sidelobe interferences, but it cannot efficiently deal with mainlobe interferences because of its only angular-dependent array factor. In contrast, FDA offers a solution to counteract mainlobe interferences. We initially discussed the functionality of FDA subarrays in suppressing mainlobe jamming signals in [42], and exploited the combination of FDA and MIMO in counteracting mainlobe jammers in [43] by jointly utilizing FDA in providing rang-dependent beampattern and MIMO in increasing degrees-of-freedom (DOFs).

Different from that in traditional radars the targets should be diagonally distributed in the transmit-receive spectral distribution due to the same transmit and receive spatial frequencies, the targets in FDA radar may be non-diagonally located in the transmit-receive spectra because of the frequency offset caused spatial frequency $\frac{2\Delta f}{c_0}r$ (see also (24)). This property can then be utilized to suppress mainlobe interferences.

After multichannel matched filtering, the FDA radar received signals can be modeled as [44]

$$\mathbf{Y} = \xi_0 \left[\mathbf{w}_T^H \mathbf{a}_\theta(\theta)\right] \mathbf{a}_r(r) \otimes \mathbf{b}(\theta) + \mathbf{a}_r(r) \otimes \mathbf{n} \tag{31}$$

where $\xi_0$ is the target reflection coefficient, $\mathbf{n}$ denotes the noise vector, $\otimes$ denotes the Kronecker product operator, and $\mathbf{a}_r(r)$ and $\mathbf{b}(\theta)$ denote the transmit steering vector in the range dimension and receive steering vector:

$$\mathbf{a}_r(r) = \left[1, e^{j\pi\Delta f\frac{4r}{c_0}}, \ldots, e^{j\pi(N-1)\Delta f\frac{4r}{c_0}}\right]^T \tag{32}$$

$$\mathbf{b}(\theta) = \left[1, e^{j2\pi f_0\frac{1}{c_0}d_r\sin\theta}, \ldots, e^{j2\pi f_0\frac{1}{c_0}(N-1)d_r\sin\theta}\right]^T \tag{33}$$

According to (31), the incoming mainlobe interference located at $(\theta_j, r_j)$ can be expressed as

$$\mathbf{Y}_j = \xi_j \left[\mathbf{w}_T^H \mathbf{a}_\theta(\theta_j)\right] \mathbf{a}_r(r_j) \otimes \mathbf{b}(\theta_j) + \mathbf{a}_r(r_j) \otimes \mathbf{n} \tag{34}$$

where $\xi_j$ denotes the incoming interference strength.

Once if the jammer and target have distinct range positions, the interference can be canceled by designing a range-related blocking matrix, even if the jammer and target are located in the same angular. Using the projection matrix:

$$\mathbf{P} = \mathbf{I} - \frac{\mathbf{a}_r(r_j)\mathbf{a}_r^H(r_j)}{\mathbf{a}_r^H(r_j)\mathbf{a}_r(r_j)} \tag{35}$$

we can get

$$\mathbf{P}\mathbf{Y}_j = \xi_j \left[\mathbf{w}_T^H \mathbf{a}_\theta(\theta_j)\right] \mathbf{P}\mathbf{a}_r(r_j) \otimes \mathbf{b}(\theta_j) + \mathbf{P}\mathbf{a}_r(r_j) \otimes \mathbf{n} = \mathbf{0}_N \tag{36}$$

This implies that the interference is successfully suppressed and the desired target with the same angle (i.e., $\theta = \theta_j$) will be preserved in the final suppressing results.

Suppose the following simulation parameters: The target and jammer are located at $(10°, 10km)$ and $(10°, 15km)$, $f_0 =$ 10 GHz, $\Delta f = 20$ kHz and $M = N = 10$, Figure 11 shows that FDA radar can suppress the mainlobe interference and detect the desired targets successfully, while phased-array radar cannot localize the target due to its range-independent transmit-receive target response.

## IV. DISCUSSIONS AND FUTURE WORKS

FDA radar can adaptively update its range-dependent beampattern in both range and azimuth dimensions to suppress space-time-range-dependent interferences. However, in the FDA radar signal processing algorithm, when the noise and interference are Gaussian, the unconstrained maximum likelihood (ML) estimate of the signal covariance matrix is actually the sample variance matrix, but it is difficult to obtain the required covariance matrix of noise and interference in the FDA radar due to its range, angle and time-dependent response. This nonstationarity results in a limited amount of snapshot data available for the processing that may be

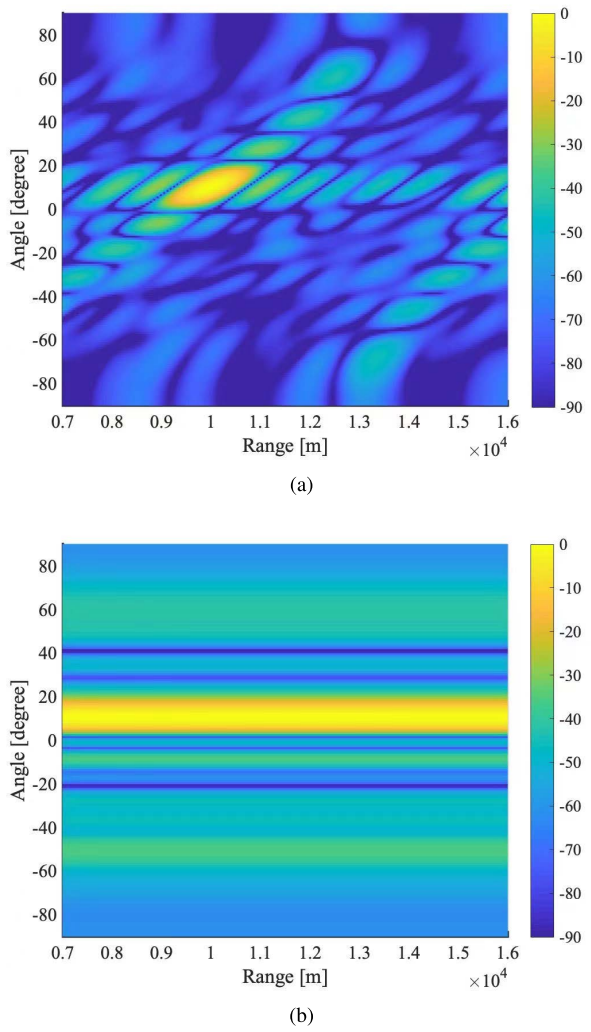


**FIGURE 11.** Mainlobe interference suppression performance: (a) FDA radar, (b) phased-array radar.

insufficient for an algorithm to coverage. A potential solution is to adopt subspace tracking algorithms such as projection approximation and fast approximated power iteration. Reiterative minimum mean square error algorithm has the capability of simultaneously adaptation in slow-time and fast-time to enhance the sensitivity by suppressing Doppler and range sidelobes, but its large computation complexity due to multidimensional adaptivity must be significantly reduced for practical engineering applications. Reduced rank techniques can reduce the rank associated with the interference-plus-noise covariance matrix. Many rank reduction methods in the literature can achieve the performance near or better than their full rank counterparts but with reduced sample support and computational load. Particularly, suboptimal fast-time STAP algorithms to suppress multipath interferences [23], while preserving the final radar detection performance, should be developed.

The basic implementation using monochromatic assumption and equally spaced elements is generally considered in the FDA literature. Many more fertile areas remain for further exploration. Linearly increasing frequency offsets and a uniform weighting vector are often assumed in existing FDA papers. However, they may be not the best choice for specific applications. Two-dimensional FDA allows three-dimensional beam-steering in the azimuth and elevation dimensions, which pattern will be extremely unique and affords additional properties to develop operational strategies. Amplitude weighting can be employed for FDA beamforming techniques, which may be also useful for rejecting multipath interferences, but more investigations are required.

Furthermore, directional modulation can be achieved for FDA. One simple approach is to divide the whole array into multiple subarrays, each of which is steered to a particular position. The frequency progression can be used across the subarrays, instead of across the elements as the basic FDA. Since the frequency progression produces both angle-dependent and time-variant beampattern, we can utilize the frequency progression in vertical dimension to alleviate the range layover effects [45]. The essence is to construct an effective and efficient mapping between the actual collection location and the apparent collection location. This is an interesting future research topic.

Another future work is to optimize the frequency offsets. It is likely that the optimized frequency allocation is actually dependent on the physical scenarios. Several methods have been studied to optimally design the frequency offsets for FDA radar (see [12] and the references wherein). It is expected that the sample support data homogeneity can be considerably increased for the targets off-boresight in azimuth, as the isodop shape is better accentuated by the FDA beampattern. It is necessary to investigate possible benefits of adaptive frequency offsets control in FDA radar systems.

Additionally, besides varying apparent angle, FDA also exhibits interesting non-uniform plane wave. This is because that, for a given range, the FDA planes of constant phase and constant amplitude do not coincide, which generates different orientations in the propagation. According to [45], the variation in FDA radar signal amplitude and phase may produce a set of apparent collection locations that are nonuniformly spaced and appear to alter the radar platform's actual moving track. An additional processing step is thus required between data collection and parameter estimation to formulate a mapping from the actual collection locations to the apparent radar collection locations. The purpose is to match the phase history collected at the actual collection locations for the FDA radar transmitted signal. In addition, the FDA radar assigned frequency offsets should operate precisely, but it is not an easy task in practical system implementation. Robust processing algorithm is necessary to address the effects of unideal frequency offsets.

## V. CONCLUSION

This paper studied FDA auto-scanning beam characteristics including range and angle coupling, beam auto-scanning rate and integral array again. Both theoretical analysis and

simulation results verify that FDA produces rather different array beam characteristics from traditional phased-array. Several potential application such as RF stealth or RF localization deception to encounter unintended interceptor, range-ambiguous clutter suppression and mainlobe interference suppression were presented to exploit FDA auto-scanning transmit beam and range-dependent transmit-receive channel response. In addition, technical challenges in space-time adaptive processing and possible future works were discussed. Certainly, it may be not possible to replace phased-array with FDA totally, as phased-arrays are prevalent today. Nevertheless, FDA can be regarded as an extension of phased-array using distinct baseband waveforms for different array elements, which can be employed to compensate the disadvantage of phased-array in range-independence and MIMO in loss of transmit array gain. It is thus believed that FDA is a promising array technique that will play an important role in radar applications.

## REFERENCES


[1] C. Mao, M. Khalily, P. Xiao, L. Zhang, and R. Tafazolli, "High-gain phased array antenna with endfire radiation for 26 GHz wide-beam-scanning applications," *IEEE Trans. Antennas Propag.*, vol. 69, no. 5, pp. 7497–7507, Nov. 2021.

[2] A. R. Vilenskiy, W.-C. Liao, R. Maaskant, V. Vassilev, O. A. Iupikov, T. Emanuelsson, and M. V. Ivashina, "Co-design and validation approach for beam-steerable phased arrays of active antenna elements with integrated power amplifiers," *IEEE Trans. Antennas Propag.*, vol. 69, no. 11, pp. 7497–7507, Nov. 2021.

[3] P. F. McManamon, P. J. Bos, M. J. Escuti, J. Heikenfeld, S. Serati, H. Xie, and E. A. Watson, "A review of phased array steering for narrow-band electrooptical systems," *Proc. IEEE*, vol. 97, no. 6, pp. 1078–1096, Jun. 2009.

[4] M. Maggi, S. Hidri, L. Marnat, M. Ettorre, G. Orozco, M. Margalef-Rovira, C. Gaquiere, and K. Haddadi, "Millimeter-wave phased arrays and over-the-air characterization for 5G and beyond: Overview on 5G mm-wave phased arrays and OTA characterization," *IEEE Microw. Mag.*, vol. 23, no. 5, pp. 67–83, May 2022.

[5] W.-Q. Wang, "Frequency diverse array antenna: New opportunities," *IEEE Antennas Propag. Mag.*, vol. 57, no. 2, pp. 145–152, Apr. 2015.

[6] W.-Q. Wang, "Ultrawideband frequency-diverse array antennas: Range-dependent and autoscanning beampattern applications," *IEEE Antennas Propag. Mag.*, vol. 60, no. 3, pp. 48–56, Mar. 2018.

[7] J. Wu, T. Wang, L. Zhang, and Z. Bao, "Range-dependent clutter suppression for airborne sidelooking radar using MIMO technique," *IEEE Trans. Aerosp. Electron. Syst.*, vol. 48, no. 4, pp. 3647–3654, Oct. 2012.

[8] B. J. Falkner, H. Zhou, A. Mehta, T. Arampatzis, M.-S. Dariush, and H. Nakano, "A circularly polarized low-cost flat panel antenna array with a high impedance surface meta-substrate for satellite on-the-move medical IoT applications," *IEEE Trans. Antennas Propag.*, vol. 69, no. 9, pp. 6076–6081, Sep. 2021.

[9] P. Mei, S. Zhang, and G. F. Pedersen, "A low-cost, high-efficiency and full-metal reflectarray antenna with mechanically 2-D beam-steerable capabilities for 5G applications," *IEEE Trans. Antennas Propag.*, vol. 68, no. 10, pp. 6997–7006, Oct. 2020.

[10] Y. Dong, Z. Wang, Y. Pan, and J. H. Choi, "Characterization of shorted dipole antennas for low-cost RFID reader applications," *IEEE Trans. Antennas Propag.*, vol. 68, no. 11, pp. 7297–7308, Nov. 2020.

[11] P. Antonik, "An investigation of a frequency diverse array," Ph.D. dissertation, Univ. College London, London, U.K., Jun. 2009.

[12] W.-Q. Wang, H. C. So, and A. Farina, "An overview on time/frequency modulated array processing," *IEEE J. Sel. Topics Signal Process.*, vol. 11, no. 2, pp. 228–246, Feb. 2017.

[13] W.-Q. Wang, "Overview of frequency diverse array in radar and navigation applications," *IET Radar, Sonar Navigat.*, vol. 10, no. 10, pp. 1001–1012, Jul. 2016.

[14] H. C. So, M. G. Amin, S. Blunt, F. Gini, and W.-Q. Wang, "Introduction of the issue on time/frequency modulated array signal processing," *IEEE J. Sel. Topics Signal Process.*, vol. 11, no. 2, p. 225, Mar. 2017.

[15] H. Bang, W.-Q. Wang, S. Zhang, and Y. Liao, "FDA-based space–time–frequency deceptive jamming against SAR imaging," *IEEE Trans. Aerosp. Electron. Syst.*, vol. 58, no. 3, pp. 2127–2140, Jun. 2022.

[16] L. Lan, M. Rosamilia, A. Aubry, A. D. Maio, and G. S. Liao, "Single-snapshot angle and incremental range estimation for FDA-MIMO radar," *IEEE Trans. Aerosp. Electron. Syst.*, vol. 57, no. 6, pp. 3705–3718, Dec. 2021.

[17] J. Xiong, W.-Q. Wang, and K. Gao, "FDA-MIMO radar range–angle estimation: CRLB, MSE, and resolution analysis," *IEEE Trans. Aerosp. Electron. Syst.*, vol. 54, no. 1, pp. 284–294, Feb. 2018.

[18] S. L. Ji, W.-Q. Wang, H. Chen, and S. S. Zhang, "On physical-layer security of FDA communications over Rayleigh fading channels," *IEEE Trans. Cognit. Commun. Netw.*, vol. 5, no. 3, pp. 476–490, Sep. 2019.

[19] S. Brady, "Frequency diverse array radar: Signal characterization and measurement accuracy," M.S. thesis, Air Force Inst. Technol., Dayton, OH, USA, May 2010.

[20] J. Huang, "Frequency diverse array: Theory and design," Ph.D. dissertation, Dept. Electron. Elect. Eng., Univ. College London, London, U.K., May 2010.

[21] M. Secmen, S. Demir, A. Hizal, and T. Eker, "Frequency diverse array antenna with periodic time modulated pattern in range and angle," in *Proc. IEEE Radar Conf.*, Boston, MA, USA, Apr. 2007, pp. 427–430.

[22] J. Huang, K.-F. Tong, and C. Baker, "Frequency diverse array: Simulation and design," in *Proc. Loughborough Antennas Propag. Conf.*, Loughborough, U.K., May 2009, pp. 253–256.

[23] C. Cetintepe and S. Demir, "Multipath characteristics of frequency diverse arrays over a ground plane," *IEEE Trans. Antennas Propag.*, vol. 62, no. 7, pp. 3567–3574, Jul. 2014.

[24] W. Khan, I. M. Qureshi, and S. Saeed, "Frequency diverse array radar with logarithmically increasing frequency offset," *IEEE Antennas Wireless Propag. Lett.*, vol. 14, pp. 499–502, 2015.

[25] Y. Liu, H. Ruan, L. Wang, and A. Nehorai, "The random frequency diverse array: A new antenna structure for uncoupled direction-range indication in active sensing," *IEEE J. Sel. Topics Signal Process.*, vol. 11, no. 2, pp. 295–308, Mar. 2017.

[26] A.-M. Yao, W. Wu, and D.-G. Fang, "Frequency diverse array antenna using time-modulated optimized frequency offset to obtain time-invariant spatial fine focusing beampattern," *IEEE Trans. Antennas Propag.*, vol. 64, no. 10, pp. 4434–4446, Oct. 2016.

[27] A.-M. Yao, W. Wu, and D.-G. Fang, "Solutions of time-invariant spatial focusing for multi-targets using time modulated frequency diverse antenna arrays," *IEEE Trans. Antennas Propag.*, vol. 65, no. 2, pp. 552–566, Feb. 2017.

[28] A.-M. Yao, P. Rocca, W. Wu, A. Massa, and D.-G. Fang, "Synthesis of time-modulated frequency diverse arrays for short-range multi-focusing," *IEEE J. Sel. Topics Signal Process.*, vol. 11, no. 2, pp. 282–294, Mar. 2017.

[29] Y. H. Xu, X. Shi, J. Xu, and P. Li, "Range-angle-dependent beamforming of pulsed frequency diverse array," *IEEE Trans. Antennas Propag.*, vol. 63, no. 7, pp. 3262–3267, Jul. 2015.

[30] M. Fartookzadeh, "Comments on 'frequency diverse array antenna using time-modulated optimized frequency offset to obtain time-invariant spatial fine focusing beampatter,'" *IEEE Trans. Antennas Propag.*, vol. 68, no. 2, pp. 1211–1212, Feb. 2020.

[31] R. Gui, B. Huang, W.-Q. Wang, and Y. Sun, "Generalized ambiguity function for FDA radar joint range, angle and Doppler resolution evaluation," *IEEE Geosci. Remote Sens. Lett.*, vol. 19, 2022, Art. no. 3502305.

[32] L. Wang, W.-Q. Wang, H. Guan, and S. Zhang, "LPI property of FDA transmitted signal," *IEEE Trans. Aerosp. Electron. Syst.*, vol. 57, no. 6, pp. 3905–3915, Dec. 2021.

[33] F. D. Lapierre, P. Ries, and J. G. Verly, "Foundation for mitigating range dependence in radar space-time adaptive processing," *IET Radar, Sonar Navigat.*, vol. 3, no. 1, pp. 18–29, Feb. 2009.

[34] J. Xu, S. Zhu, and G. Liao, "Space-time-range adaptive processing for airborne radar systems," *IEEE Sensors J.*, vol. 15, no. 3, pp. 1602–1610, Mar. 2015.

[35] T. Higgins, "Waveform diversity and range-couple adaptive radar signal processing," Ph.D. dissertation, Dept. Elect. Eng. Comput. Sci., University of Kansas, Lawrence, KS, USA, 2011.

[36] J. Xu, G. Liao, L. Huang, and H. C. So, "Robust adaptive beamforming for fast-moving target detection with FDA-STAP radar," *IEEE Trans. Signal Process.*, vol. 65, no. 4, pp. 973–984, Feb. 2017.

[37] C. Wen, J. Peng, Y. Zhou, and J. Wu, "Enhanced three-dimensional joint domain localized STAP for airborne FDA-MIMO radar under dense false-target jamming scenario," *IEEE Sensors J.*, vol. 18, no. 10, pp. 4154–4166, May 2018.
[38] C. Wen, Y. Huang, J. Peng, J. Wu, G. Zheng, and Y. Zhang, "Slow-time FDA-MIMO technique with application to STAP radar," *IEEE Trans. Aerosp. Electron. Syst.*, vol. 58, no. 1, pp. 74–95, Feb. 2022.
[39] J. Xu, S. Zhu, and G. Liao, "Range ambiguous clutter suppression for airborne FDA-STAP radar," *IEEE J. Sel. Topics Signal Process.*, vol. 9, no. 8, pp. 1620–1631, Dec. 2015.
[40] R. Klemm, *Principles of Space-Time Adaptive Processing*. London, U.K.: IEEE Press, 2002.
[41] C. Schleher, *MTI and Pulsed Doppler Radar With MATLAB*. Norwood, MA, USA: Artech House, 2010.
[42] G. Liu, H. Huang, and W.-Q. Wang, "Frequency diverse array radar in counteracting mainlobe jamming signals," in *Proc. IEEE Radar Conf. (RadarConf)*, Seattle, DC, USA, May 2017, pp. 1–5.
[43] W.-Q. Wang, H. C. So, and A. Farina, "FDA-MIMO signal processing for mainlobe jammer suppression," in *Proc. 27th Eur. Signal Process. Conf. (EUSIPCO)*, Sep. 2019, pp. 1–5.
[44] R. H. Gui, W.-Q. Wang, C. Cui, and H. C. So, "Coherent pulsed-FDA radar receiver design with time-variance consideration: SINR and CRB analysis," *IEEE Trans. Signal Process.*, vol. 66, no. 1, pp. 200–214, Jan. 2018.
[45] J. Farooq, "Frequency diversity for improving synthetic aperture radar imaging," Ph.D. dissertation, Air Force Inst. Technol., Dayton, OH, USA, 2009.

**WEN-QIN WANG** (Senior Member, IEEE) received the B.E. degree in electrical engineering from Shandong University, Shandong, China, in 2002, and the M.E. and Ph.D. degrees in information and communication engineering from the University of Electronic Science and Technology of China (UESTC), Chengdu, China, in 2005 and 2010, respectively.

From March 2005 to 2007, he was with the National Key Laboratory of Microwave Imaging Technology, Chinese Academy of Sciences, Beijing, China. Since September 2007, he has been with the School of Information and Communication Engineering, UESTC, where he is currently a Professor and the Director. From June 2011 to May 2012, he was a Visiting Scholar with the Stevens Institute of Technology, Hoboken, NJ, USA. From December 2012 to December 2013, he was a Hong Kong Scholar with the City University of Hong Kong, Hong Kong. From January 2014 to January 2016, he was a Marie Curie Fellow with the Imperial College London, U.K. His research interests include signal processing for radar, communications, and microwave remote sensing. He was a recipient of the Marie Curie International Incoming Fellowship, the National Young To-Notch Talent of the Ten-Thousand Talent Program Award, and the Hong Kong Scholar Fellowship. He is an editorial board member of four international journals.